1 **Mass spectral characterization of secondary organic aerosol from urban**

2 **lifestyle sources emissions**

3 Wenfei Zhu[1], Song Guo[1,2*], Min Hu[1], Zirui Zhang[1], Hui Wang[1], Ying Yu[1], Zheng Chen[1], Ruizhe Shen[1], Rui

4 Tan[1], Kai Song[1], Kefan Liu[1], Rongzhi Tang[1], Yi Liu[1], Shengrong Lou[3], Yuanju Li[1], Wenbin Zhang[4], Zhou

5 Zhang[4], Shijin Shuai[4], Hongming Xu[4], Shuangde Li[5], Yunfa Chen[5], Francesco Canonaco[6], Andre. S. H.

6 Prévôt[6]

7 *[1] State Key Joint Laboratory of Environmental Simulation and Pollution Control, International Joint Laboratory for*

8 *Regional Pollution Control, Ministry of Education (IJRC), College of Environmental Sciences and Engineering, Peking*

9 *University, Beijing 100871, China P. R.*

10 *[2] Collaborative Innovation Center of Atmospheric Environment and Equipment Technology, Nanjing University of*

11 *Information Science & Technology, Nanjing 210044, China P. R.*

12 *[3] State Environmental Protection Key Laboratory of Formation of Urban Air Pollution Complex, Shanghai Academy of*

13 *Environmental Sciences, Shanghai 200233, China P. R.*

14 *[4] State Key Laboratory of Automotive Safety and Energy, Tsinghua University, Beijing 100084, China P. R.*

15 *[5] State Key Laboratory of Multiphase Complex Systems, Institute of Process Engineering, Chinese Academy of Sciences,*

16 *Beijing 100190, China P. R.*

17 *[6] Laboratory of Atmospheric Chemistry, Paul Scherrer Institute (PSI), Villigen 5232, Switzerland*

18

19 Corresponding authors:

20 *Song Guo − State Key Joint Laboratory of Environmental Simulation and Pollution Control, College of

21 Environmental Sciences and Engineering, Peking University, Beijing 100871, China P. R.; Email:

22 songguo@pku.edu.cn

23

24 **Abstract** In the present work, we conducted experiments of secondary organic aerosol (SOA) formation from urban

25 lifestyle sources (cooking and vehicle) to characterize the mass spectral features of primary organic aerosol (POA) and SOA

26 using an high-resolution time-of-flight aerosol mass spectrometer (HR-ToF-AMS). Our results showed that the cooking

27 styles have greater impact on aged COA mass spectra than oxidation condition. However, the oxidation conditions affect the

28 aged HOA spectra more significantly than vehicle operation conditions. In our study, we use mass spectra similarity

29 analysis and positive matrix factorization (PMF) analysis to establish the POA and SOA mass spectra of these two typical

Atmospheric
Chemistry
and Physics
Discussions

30 lifestyle sources. These mass spectra are used as source constraints in a multilinear engine (ME-2) model to apportion the

31 OA sources in the atmosphere. Comparing with the traditional ambient PMF results, the improved ME-2 model can better

32 quantify the contribution of POA and SOA from life-style sources. Our work, for the first time, establishes the vehicle and

33 cooking SOA source profiles, and can be further used in the OA source apportionment in the ambient atmosphere.

34

35
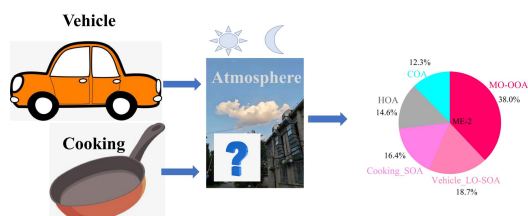
1. Introduction

37 Organic aerosol (OA) is an important component of fine particulate matter and has significant

38 environmental and health effects, especially in the urban areas (Guo et al., 2012; Guo et al., 2014; Ying et al.,

39 2020). Currently, real-time measurements of OA based on the aerosol mass spectrometer (AMS) has become

40 an effective way to explore OA characteristics in the field campaigns and laboratory studies (Canagaratna et

41 al., 2007; Ge et al., 2017; Hu et al., 2016a; Huang et al., 2011; Kim et al., 2017; Li et al., 2017; Sun et al.,

42 2016; Zhang et al., 2011). Applying positive matrix factorization (PMF) and a multilinear engine (ME-2)

43 (Paatero, 1999) to analyze the high-resolution mass spectrometry fragments, OA can be further identified as

44 primary organic aerosol (POA) and secondary organic aerosol (SOA). POA includes vehicle exhaust

45 (precisely, a kind of hydrocarbon-like OA, HOA), cooking (COA) and biomass burning (BBOA), which

46 SOA includes low oxygenated OA (LO-OOA) and more oxygenated OA (MO-OOA)(Canonaco et al., 2013;

47 Elser et al., 2016; Qin et al., 2017; Zhang et al., 2017a; Zhou et al., 2018). As lifestyle sources in urban,

48 cooking and vehicle emissions, that is COA and HOA mostly determine ambient OA loadings. For example,

49 primary cooking OA (COA) and vehicle exhaust OA (HOA) accounted for 10-35 % and 6-26% of OA,

50 respectively, in urban areas in China (He et al., 2011; Hu et al., 2017; Sun et al., 2010; Sun et al., 2014; Sun

51   et al., 2018; Wang et al., 2016; Xu et al., 2016; Zhang et al., 2014).

52   Besides the contribution to POA, many studies have found that these two typical urban lifestyle sources

53   may also emit a large number of volatile organic compounds (VOCs) (Katragadda et al., 2010; Klein et al.,

54   2016), semi-volatile organic compounds (SVOCs), and intermediate volatile organic compounds (IVOCs)

55   ($\geqslant$ C13n-alkanes and fatty acids) (Louvaris et al., 2017; Schauer et al., 2002) ,which may also play

56   important roles in SOA formation. However, based on collocated AMS measurements and factor analysis

57   results, the SOA formed by vehicle and cooking sources cannot be effectively resolved from the total SOA

58   due to the lack of secondary mass spectral profiles. The POA mass spectral profiles based on AMS including

59   HOA (Collier et al., 2015), BBOA (Alfarra et al., 2007; He et al., 2010; Xu et al., 2020), and COA (He et al.,

60   2010; Liu et al., 2017; Mohr et al., 2012; Xu et al., 2020) have been fully explored in laboratory studies, and

61   applied as constraint factors into the ME-2 model in the ambient air. Some studies have made it possible to

62   quantify biogenic secondary aerosol products of a single precursor, such as isoprene oxidation products

63   (IEPOX)(Budisulistiorini et al., 2013; Hu et al., 2016b), and have been extended to the urban atmosphere to

64   obtain an IEPOX-SOA factor via PMF analysis of OA spectra(Zhang et al., 2017b). Although several studies

65   explored the mass spectral characteristics of SOA from anthropogenic life-style sources, i.e., heated cooking

66   oils, gasoline motors, and diesel engines (Kaltsonoudis et al., 2017; Liu et al., 2018; Presto et al., 2014), the

67   spectral profiles of cooking SOA under actual cooking conditions and vehicle SOA under different emission

68   conditions are still uncertain. Besides, to date, studies that used ME-2 for a better anthropogenic SOA source

69   apportionment by inputting their SOA spectra as constraints remain scarce. Therefore, the mass spectra of

70   SOA from abundant anthropogenic life-style sources are urgent to characterize for conducing to acquire a

71   better source apportionment of SOA.

72   In this work, cooking and vehicle experiments were carried out to investigate the variation in mass

73   spectra profiles of POA and SOA from Chinese cooking emissions under different cooking styles and

74 vehicle emissions under different running conditions using high-resolution time-of-flight AMS

75 (HR-ToF-AMS). The mass spectral characterizations of POA and SOA from cooking and vehicle emissions

76 were intercompared, and their changes in some indicated ionic fragments were elucidated. Besides, we

77 verified the mass spectral profiles by applying mass spectra of POA and SOA to ME-2 for source

78 apportionment of OA in the winter observation with various primary emissions and the summer observation

79 with high oxidation conditions.

80 **2. Materials and Methods**

81 **2.1 Simulation of POA emission and SOA formation from urban lifestyle sources.**

82 For cooking, we prepared four dishes including deep-frying chicken, shallow-frying tofu, stir-frying

83 cabbage, and Kung Pao chicken. The fumes produced by cooking were introduced into the Gothenburg

84 Potential Aerosol Mass (Go: PAM) reactor (Li et al., 2019) after being diluted 8 times by a Dekati Dilutor

85 (e-Diluter, Dekati Ltd., Finland). We considered the emissions sampled after Go: PAM without OH radical

86 as primary emissions, and those measured after Go: PAM with the given OH exposure as secondary

87 formation. In addition, the background blank groups and the dilution gas blank groups were separately

88 completed using boiling water and dilution gas, according to the same steps as experimental groups. More

89 information of experimental setup of cooking simulations can be found in Zhang et al., 2020 (Zhang et al.,

90 2020). For vehicle, experiments were performed by using GDI engine with a commercial China V gasoline

91 fuel (Emission: 998cc; Maximum power: 100KW 6000rpm; Peak torque: 205Nm 2000-3000rpm). Five

92 running conditions covering different speeds and torques, including 1500rpm_16Nm, 1750rpm_16Nm,

93 2000rpm_16Nm, 2000rpm_32Nm, and 2000rpm_40Nm, were used to characterize their POA and SOA mass

94 spectra. We adjusted input ozone concentration ranging from ~0 to ~7.7 ppm to change the OH exposure in

95 the Go: PAM.

96 **2.2 Instrumentation and data analysis.**

97 **Figure S1** shows the schematic of the experimental system. Two scanning mobility particle sizers

98 (SMPS-1, Electrostatic Classifier model 3080, Condensation Particle Counter model 3778; SMPS-2,

99 Electrostatic Classifier model 3082, Condensation Particle Counter model 3772; TSI Incorporation, USA)

100 were set at the inlet and outlet of Go: PAM to correct the wall loss. The size distribution and number

101 concentration of particles were scanned every 2 (cooking) - 5 min (vehicle) before and after Go: PAM for

102 cooking and vehicle experiment, respectively. The chemical compositions and high-resolution ions

103 fragments of OA were measured by an aerodyne high-resolution time-of-flight aerosol mass spectrometer

104 (HR-ToF-AMS, Aerodyne Research Incorporation, USA), synchronize with SMPS.

105 Before and after the two experiments, the ionization efficiency (IE) of HR-ToF-AMS IE calibrations

106 were carried out by using 300 nm mono-dispersed ammonium nitrate particles combining with SMPS. The

107 collection efficiency (CE) of HR-ToF-AMS was obtained from comparing AMS and synchronous SMPS

108 real-time measurement of particle mass concentrations at the outlet of Go: PAM. Besides, the CO_2

109 concentrations were simultaneously measured using a CO_2 analyzer (Model 410i, Thermo Electron

110 Corporation, USA) to reduce the CO_2 interference to organic fragments in mass spectra. Other gas phase

111 measurements included carbon monoxide (CO, Thermo, Model 48i TL), NO_x (Thermo, Model 42i TL) and

112 SO_2 (Thermo, Model 42i TL).

113 The mass concentration, size distribution and the ion-speciated mass spectra of NR-PM$_1$ species were

114 analyzed using the HR-ToF-AMS standard data analysis software (SQUIRREL version 1.57 and PIKA

115 version 1.16). In this study, we used the igor-based PMF model with PMF2.exe algorithm (Paatero and

116 Hopke, 2003) and the PMF Evaluation Toolkit version 2.08D (Ulbrich et al., 2009) to separate the POA and

117 SOA from aged cooking and vehicle organic aerosol, following the procedure presented in the literatures

118 (Hu et al., 2016a; Zhang et al., 2011). The OH exposure and equivalent photochemical age (EPA) were

119 calculated by off-line methods according to SO_2 decay shown in Zhang et al., 2020 (Zhang et al., 2020),

120 which were validated by a flow reactor exposure estimator using measured concentrations of reactive

121 compounds such as VOCs, CO and NO_x (Peng et al., 2016). The OH exposure and photochemical age for all

122 conditions in cooking and vehicle experiments were listed in **Table S1**.

123 **2.3 Mass spectra similarity analysis.**

124 In this study, the angle θ was used to evaluate the correlation between the two AMS mass spectra

125 features. The angle θ between the two AMS mass spectra (MSa, MSb) is given by:

126
$$\cos\theta = \frac{\text{MSaMSb}}{|\text{MSa}||\text{MSb}|}$$

127 The θ angle between two mass spectra is 0-5, 5-10, 10-15, 15-30, and > 30, which means excellent

128 consistency, good consistency, many similarities, limited similarities, and poor consistency, respectively,

129 (Kaltsonoudis et al., 2017; Kostenidou et al., 2009).

130 **3. Results and Discussion**

131 **3.1 Mass spectra of POA and aged OA from the life style sources.**

132 **Fig.1a** shows the mass spectra of aged HOA under different vehicle running conditions when EPA was

133 0.6 days. The mass spectra of aged HOA emission from different vehicle running conditions under other

134 various oxidation degrees are included in **Fig.S2**. All the aged HOA spectral profiles from different vehicle

135 running conditions showed a similar pattern. and the θ angles among the mass spectra of aged HOA were

136 less than 10° at EPA 0.6 days (**Table 1**), suggesting a little difference between the mass spectra. The mass

137 spectra of aged HOA at 0.6 days were dominated by the ion series of $C_nH^+_{2n+1}$ (m/z 29, 43, 57, 71, 85...) and

138 $C_nH_{2n-1}^+$ (m/z 41, 55, 69, 83...), resulting from less oxidized components such as saturated alkanes, alkenes.

139 As the highest proportion of ion fragments, m/z 43 and 29 consisted of oxygen-containing ions like CHO^+

140 and $C_2H_3O^+$, respectively, whose fractions were much larger than the hydrocarbon-like ion fragments at the

141 same mass integers. Besides, there were also abundant tracer ion fragments for SOA (m/z 28 and m/z 44).

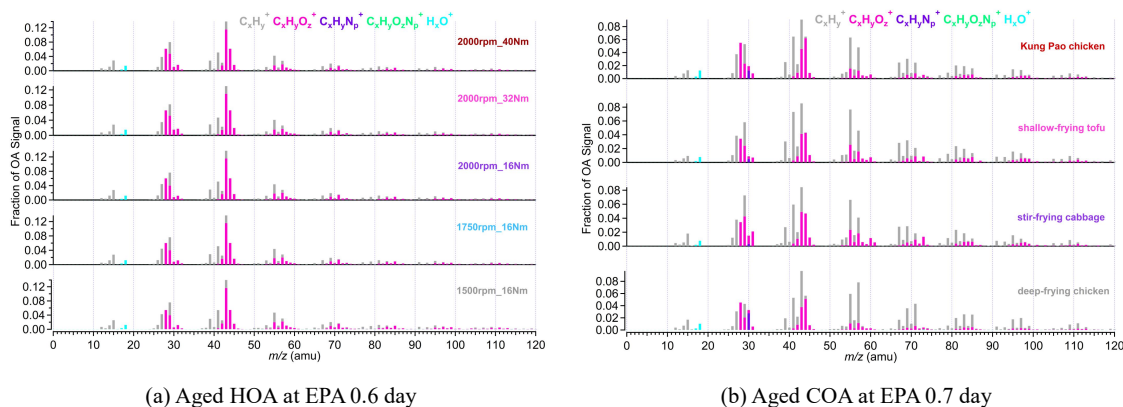(a) Aged HOA at EPA 0.6 day   (b) Aged COA at EPA 0.7 day

Fig.1. (a) The mass spectra of aged HOA emission from different vehicle running conditions at EPA 0.6 day; (b) The mass spectra of aged COA from four Chinese dishes at EPA 0.7 day. Five running conditions covers different speeds and torques, including 1500rpm_16Nm, 1750rpm_16Nm, 2000rpm_16Nm, 2000rpm_32Nm, and 2000rpm_40Nm. Four dishes include deep-frying chicken, shallow-frying tofu, stir-frying cabbage, and Kung Pao chicken.

142

143   The mass spectra of aged COA at 0.7 days of EPA are presented in **Fig.1b**. Detailed mass spectra of

144 aged COA under other various oxidation degrees are included in **Fig.S3**. The similarity of aged COA among

145 different types of cooking were greater that of aged HOA among different running conditions when the EPA

146 was at the same level. Except for the θ angles of deep-frying chicken vs stir-frying cabbage (21°), and

147 deep-frying chicken vs shallow-frying tofu (19°), the θ angles among other aged COA at EPA 0.7 day

148 exhibited good agreement (θ<15°) in mass spectra (**Table 1**). The mass spectra of cooking were dominated

149 by the similar ion series as those of vehicle, which were mostly m/z 28, m/z 29, m/z 41, m/z 43, m/z 44, m/z

150 55, m/z 57, m/z 67, and m/z 69. However, the major mass spectral differences between cooking and vehicle

151 were the abundance of m/z 41 and the ratio of oxygen-containing ions to hydrocarbon ions ($C_xH_yO_z^+/C_xH_y^+$).

152 The four Chinese dishes had prominent peaks at m/z 41, m/z 43 and m/z 55 (generated from $C_3H_5^+$ and

153 $C_3H_7^+$, $C_4H_7^+$) which was qualitatively consistent with mass spectra of primary COA in other studies (Xu et

154 al., 2020). As described by He et al. (2010), the most abundant ion fragments at m/z 41 and m/z 55 from

155 primary Chinese cooking emissions are resulting from unsaturated fatty acids (He et al., 2010).

156   Table 1 The θ angles among the mass spectra of (a) aged HOA at EPA 0.6 day and (b) aged COA at EPA 0.7 day

(a)

Atmospheric
Chemistry
and Physics
Discussions

θ angles	1500rpm_16Nm	1750rpm_16Nm	2000rpm_16Nm	2000rpm_32Nm	2000rpm_40Nm
1500rpm_16Nm	0	3	3	8	4
1750 rpm_16 Nm		0	0.1	5	3
2000 rpm_16 Nm			0	5	3
2000 rpm_32 Nm				0	4
2000 rpm_42 Nm					0

157

(b) θ angles	deep-frying chicken	stir-frying cabbage	shallow-frying tofu	Kung Pao chicken
deep-frying chicken	0	21	19	14
stir-frying cabbage		0	10	13
shallow-frying tofu			0	12
Kung Pao chicken				0

158

159   **Fig.2a** shows the mass spectra of aged HOA oxidation at different OH exposures under the same

160   vehicle running condition (2000rpm, 16Nm). The changes in mass spectra of aged HOA under different

161   conditions are provided in **Fig.S4**. As the oxidation degree increased, the ion fragments varied similarly with

162   hydrocarbon-like ion fragments decreasing. The mass spectra at 2.89 days and 4.15 days had very similar

163   patterns with the most prominent peaks at m/z 28 and 44, respectively, which almost resembled the mass

164   spectra of MO-OOA resolved from ambient datasets. When EPA was 1.65 days, there were different mass

165   spectra patterns with dominant signals at m/z 28 and m/z 44, yet contained a large signal at m/z 43, similar

166   to the spectra of the ambient LO-OOA. Oxidation degrees greatly affected the similarity of mass spectra

167   between POA and those of aged HOA. The mass spectra profile of vehicle POA displayed poor agreement

168   (θ > 30°) with all aged HOA spectra profiles (**Tables S4-S5**). Besides, the mass spectra under the low

169   oxidation degree (EPA was 0.6 day) was also poorly correlated with those mass spectra under the high

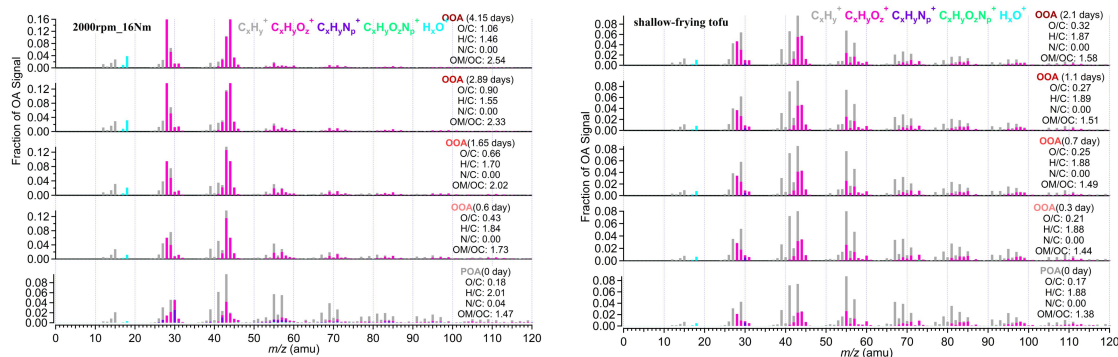170   oxidation degree (EPA were 2.89 and 4.15 days).

Fig.2. (a) The mass spectra of aged HOA oxidation of different OH exposure under the same vehicle emission condition (2000rpm, 16Nm). (b) The mass spectra of aged HOA oxidation of different OH exposure for shallow-frying tofu. The OH exposure and equivalent photochemical age (EPA) were calculated by off-line methods according to SO_2 decay shown in Table S1.

171

172   The mass spectra of primary COA and aged COA showed great inter-correlations ($\theta < 15°$), which were

173   smaller than that of vehicle OA (**Table S4-S5**). Along with the growth of OH exposure, the f_{43} of aged COA

174   increased from 0.07 to 0.10, and meanwhile its $f44$ increased from 0.03 to 0.08 (**Fig.2b; Fig.S5**),

175   distributing in the lower region of less oxidized organic aerosol (LO-OOA). The spectra of these aged COA

176   derived herein displayed almost the same variation with those of cooking oils OA (Liu et al., 2018). It

177   should be noted that the fractions of m/z 28 and m/z 44 signals in aged COA were lower than those of aged

178   HOA at the similar EPA. In addition, the aged COA had more hydrocarbon-like ions at the same mass

179   integers than aged HOA.

180   All the above results imply that oxidation condition drives the variabilities in mass spectra of the

181   vehicle OA. In contrast, cooking styles instead of oxidation conditions, significantly affected the mass

182   spectra of cooking OA. Here we concluded some possible explanations for these results. On one hand, under

183   the same oxidation conditions and different emission conditions, the similarity among the mass spectra of

184   vehicles was larger than that of cooking, which may be related to their precursors. Some studies have shown

185   that the species and the proportion of gaseous organic matter emitted by different dishes are quite different

186   (Wang et al., 2018). As described in the literature, alkanes and O-VOCs contributed to over 97% of the total

187   VOCs for fried food, and O-VOCs were the dominant contributors for Sichuan and Hunan cuisine where

188   stir-frying is common (Wang et al., 2018). Different gaseous precursors cause distinctions in the particle

189   phase SOA formation, which is reflected in the variations of AMS ion fragments between four dishes in our

190   study. Compared to cooking, the precursors from vehicles are mainly hydrocarbons, and the difference in

191   emissions under different running conditions is inapparent (Robinson et al., 2007). On the other hand, under

192   the same emission conditions and different oxidation conditions, the similarity among the mass spectra of

193   cooking sources is larger than that of vehicle sources, likely due to the oxidation pathway of precursors. As

194   mentioned above, O-VOCs are important precursors of cooking sources, and their oxidation mechanisms is

195   mostly alcohol/peroxide substitution process. This conclusion was proved by a Van Krevelen diagram,

196   showing that the cooking data gather around the slope of approximately -0.1 (Zhang et al., 2020), in

197   agreement with that of heated oils OA (Liu et al., 2018). However, for vehicles, with the increase of

198   oxidation degrees, the reaction pathways of hydrocarbon precursors varied diversely. In Van Krevelen space,

199   the vehicle data fell along a line with a slope of -0.5 (**Fig.S6**), indicating oxidation processes involving the

200   addition of both carboxylic acid and alcohol or peroxide functional groups without fragmentation and/or the

201   addition of carboxylic acid functional groups with fragmentation.

202   **3.2 Identification of the life style sources SOA mass spectra.**

203   The high abundance of m/z 41, 55, and 57 in aged COA mass spectra may be a sign that aged OA

204   identified in this study is a mixture of POA and SOA. PMF analysis was performed on the high-resolution

205   mass spectra to split SOA and POA factors from aged COA. Similarly, the same PMF procedure was also

206   applied for vehicle datasets.

207   Some ions like m/z 41, 55, 57, 43, 28, and 44 are typically used as tracers of OOA, COA, HOA,

208   LO-OOA and MO-OOA. **Fig.3** shows the high-resolution mass spectra of POA and SOA from four Chinese

209   dishes and five vehicle running conditions. The cooking POA of four Chinese dishes all showed obvious

210   hydrocarbon-like features with a large abundance of f_{57}, f_{55}, or f_{41} (fraction of m/z 57, 55 and 41 in OA,

211   respectively). For all experiments, the prominent peaks of cooking POA were m/z 41 (f_{41}=0.051~0.069), 43

212   (f_{43}=0.068~0.083), 55 (f_{55}=0.064~0.084), 57 (f_{57}=0.041~0.097), 67 (f_{67}=0.021~0.40), 69 (f_{69}=0.034~0.049)

213   dominated by $C_3H_5^+$, $C_3H_7^+$, $C_4H_7^+$, $C_4H_9^+$, $C_5H_7^+$ and $C_5H_9^+$ respectively. It was observed that fractions of

214   oxygen-containing ions were rising while those of hydrocarbon-like ions were declining during the

215   oxidation process. As for mass spectra of cooking SOA, the fractions of oxygen-containing ions were higher

216   than those of hydrocarbon-like ions. The prominent peaks were m/z 28 (f_{28}=0.045~0.068), 29

217   (f_{29}=0.048~0.080),   41   (f_{41}=0.050~0.068),   43   (f_{43}=0.087~0.103),   44   (f_{44}=0.058~0.080),   55

218   (f_{55}=0.050~0.064) and 57 (f_{57}=0.036~0.067), dominated by CO^+, CHO^+, $C_2H_5^+$ $C_3H_7^+$, $C_2H_3O^+$, CO_2^+,

219    $C_3H_5^+$, $C_4H_7^+$, $C_3H_3O^+$, $C_4H_9^+$ and $C_3H_5O^+$ respectively. The evolution of m/z 43 from POA to SOA revealed

220   a larger fraction and enhancement than those of m/z 44, suggesting that the domestic cooking SOA may

221   generate from a less oxidized process.

222   Different from the cooking, two OOA factors were derived from vehicle SOA due to higher OH

223   exposure. According to different O/C ratios, they were considered to be low oxidized vehicle SOA

224   (LO-SOA) and more oxidized vehicle SOA (MO-SOA). As indicated in **Fig.3**, the prominent m/z 28

225   (average f_{28}=0.045), 41 (average f_{41}=0.046), 43 (average f_{43}=0.158),44 (average f_{44}=0.054), 55 (average

226   f_{55}=0.039), 57 (average f_{57}=0.027) were comparable with those of cooking SOA. The fraction of m/z 43 of

227   LO-SOA was higher than that in cooking SOA by a factor of 2. The abundant m/z 28 and 44 (mainly

228   generated from CO_2^+) are widely used as the ambient MO-OOA markers.(Sun et al., 2018; Xu et al., 2017).

229   We observed high factions of m/z 28 (f_{28}=0.110~0.214) and m/z 44 (f_{44}=0.121~0.224) in MO-SOA and high

230   O/C ratios (0.88~1.33), which were much higher than those of LO-SOA (O/C=0.37~0.53) and cooking SOA

231   (O/C=0.29~0.41).

Atmospheric
Chemistry
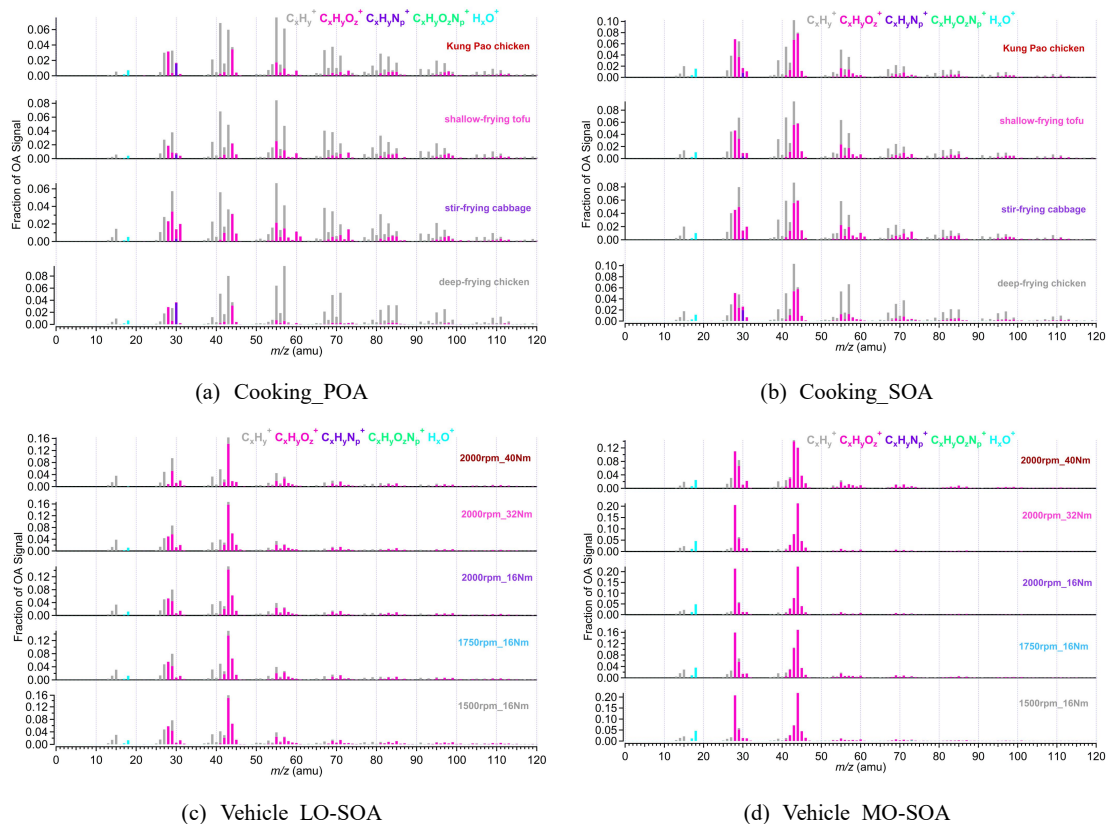and Physics
Discussions

Open Access

EGU

Fig.3. The mass spectra of PMF-POA and SOA from vehicle and cooking. PMF analysis was performed on the high-resolution mass spectra to split two factors (cooking POA and SOA) from aged COA and two SOA factors (vehicle LO-SOA and MO-SOA) from aged HOA, respectively.

232

Similarly, for the resolved SOA factor, the correlation of mass spectra among cooking groups under different cooking methods (θ = 8~21°) was worse than that of vehicle groups (θ = 3~7°) under different running conditions (**Table S8; Table S10**). The mass spectra of the PMF POA factors for deep-frying chicken exhibited poor agreement with those of stir-frying cabbage, Kung Pao chicken, and shallow-frying tofu (**Table S9**). In addition, we also found that the θ angles between LO-OOA and MO-OOA under five GDI running conditions were ranged from 36° to 50° (**Fig.S7**), indicating that the mass spectra profiles of LO-OOA are much different from those of MO-SOA, consistent with the changes in the mass spectra characteristics of vehicles, under the same emission conditions and different oxidation conditions. Our

241 results suggest that it is necessary to consider the cooking styles when constraining cooking and atmospheric

242 oxidation conditions when constraining vehicle factors.

3.3 Application of established POA and SOA profile in ambient OA source apportionment.

244 Based on the similarity analysis results of the four cooking groups, the mass spectra of deep-frying

245 chicken were poorly correlated with the others. Therefore, taking into account the cooking methods of

246 Chinese dishes, PMF model was used to identify the POA and SOA of the cooking as the primary and

247 secondary spectrum constraints for ME-2 by combining the high-resolution mass spectra datasets of the

248 three dishes except for deep-frying chicken. Similarly, combining different GDI running conditions,

249 LO-SOA and MO-SOA which were resolved based on PMF model were used as the inputting mass spectra

250 profiles of vehicles for ME-2 (**Fig.S8**).

251 The θ angles between the mass spectral profiles from urban lifestyle sources and ambient

252 PMF-resolved factors were calculated and summarized in **Fig.4** and **Table S11**. The AMS mass spectra of

253 ambient factors were obtained in Shanghai, Dezhou, Beijing, and Shenzhen in China (Hu et al., 2017;

254 Wenfei et al., 2020). The θ angles among ambient COA, HOA, LO-OOA and MO-OOA factors and the

255 cooking PMF POA, SOA, and the vehicle PMF LO-SOA, MO-SOA were ranged from 18° to 52° (**Fig.4**),

256 suggesting that the cooking PMF POA, SOA, and the vehicle PMF LO-SOA, MO-SOA can be used as

257 source constraints for ME-2 in ambient air.

13

Fig.4. The θ angles between ambient COA, HOA, LO-OOA and MO-OOA factors and the cooking PMF POA, SOA, and the vehicle PMF LO-SOA, MO-SOA. The θ angle between two mass spectra is 0-5, 5-10, 10-15, 15-30, and > 30 indicates excellent consistency, good consistency, many similarities, limited similarities, and poor consistency, respectively.

258

259   Considering the actual oxidation conditions or the concentration of OH radicals, the cooking PMF POA,

260   SOA, and the vehicle PMF LO-SOA was finally selected as the input source spectra of ME-2. We further

261   demonstrated the feasibility of input primary and secondary mass spectra for OA source apportionment in

262   two field campaigns at urban site of Shanghai in summer and winter. Ambient PMF-resolved OA factors

263   included POA factors i.e., HOA, COA, and SOA factors i.e., LO-OOA and MO-OOA in the summer and

264   winter observations in Shanghai. The HOA and COA identified by PMF contributed as high as 16 % and

265   26 % to OA in the winter observation, respectively, far exceeding expectations (**Fig.5**). In addition, the

266   ME-2 source analysis was performed by using two primary OA factors (the cooking PMF POA, HOA

267   resolved in three cities) and two secondary OA factors (the cooking PMF SOA, the vehicle PMF LO-SOA)

268   as constraints based on the same ambient OA datasets as PMF model during the summer and winter

269   observations of Shanghai.

270

14

271

272
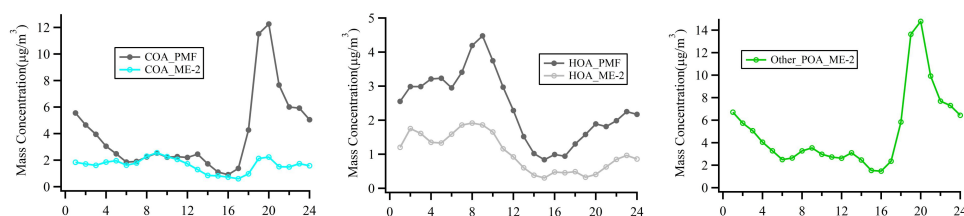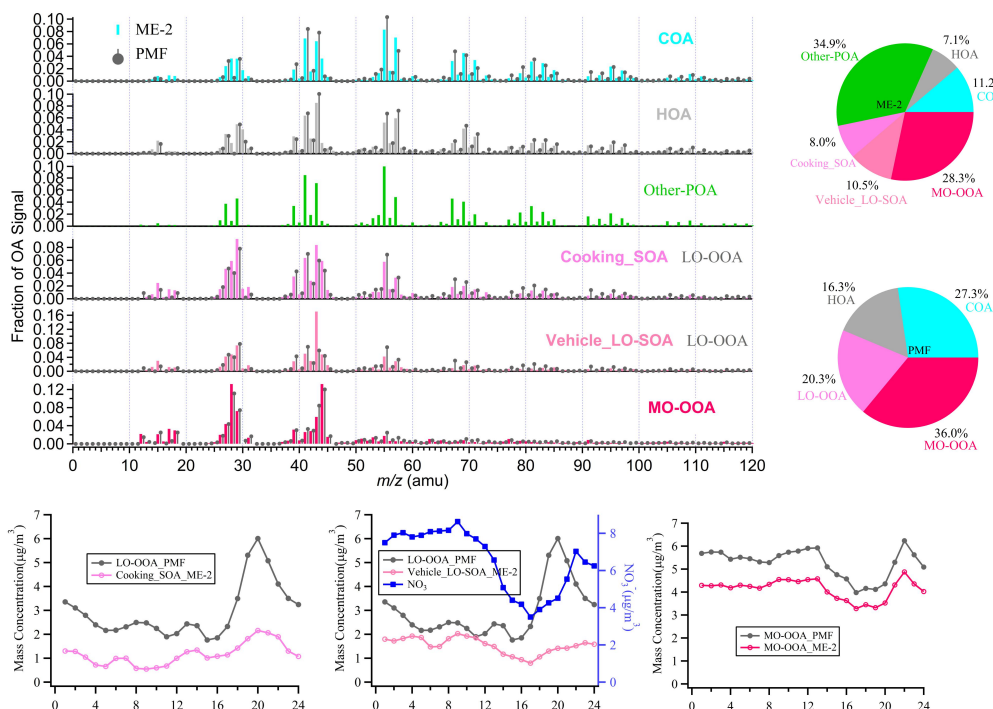
Fig.5. The comparison of the mass spectra, the diurnal variation, and fraction between ME-2 and PMF resolved factors during the wintertime in Shanghai. The black lines in the spectra and diurnal pattern are the result of PMF analysis of the actual atmosphere in Shanghai winter. The others correspond to the ME-2 source analysis results by using two primary OA factors (the cooking PMF POA, HOA resolved in three cities) and two secondary OA factors (the cooking PMF SOA, the vehicle PMF LO-SOA) as constraints based on the same ambient OA datasets as PMF model during the summer observations of Shanghai.

279

As shown in **Fig.5**, compared with PMF results, the proportions of HOA (7%) and COA (11%) obtained by source apportionment with ME-2 have significantly decreased during the winter observation. As expected, other POA contributions were identified in the highly polluted season, consistent with influences from biomass burning and coal combustion emissions. The diurnal patterns of PMF factors and ME-2 factors were consistent with the corresponding tracers during the winter observation. We noticed that the vehicle SOA analyzed by ME-2 exhibited more consistence with the diurnal variation of nitrate, especially the reasonable peak disappears at night, which shows that the LO-OOA mixed with POA is well separated by using ME-2 in winter. For the source apportionment in summer (**Fig S8**), the fraction of COA reduced

288 from 21% (PMF result) to 12% (ME-2 result). As a primary emission source with a stable contribution, COA

289 based on ME-2 analysis accounted for the same proportion of OA in summer as in winter. Moreover, the

290 diurnal patterns of ME-2 SOA factors present more reasonable than PMF SOA factors. For example, the

291 MO-OOA obtained based on ME-2 analysis was in good agreement with the diurnal variation of O_x in

292 summer, which better reflects the characteristics of the MO-OOA factor. In general, the accurate source

293 apportionment results have significant indicated that the reliability source profiles of the primary and

294 secondary of cooking and vehicles obtained in our study can be used as constraint for source apportionment

295 of OA with ME-2.

296 4. **Conclusions and Implication**

297   POA emissions, and SOA formation in PAM reactor from urban lifestyle sources were explored. The

298 aged COA had higher hydrocarbon ions than aged HOA in mass spectra. Based on the mass spectra of these

299 two urban lifestyle sources derived from the lab simulation, the ME-2 source apportionment in Shanghai

300 suggest that the reasonable of the primary and secondary source profiles of cooking and vehicles were

301 obtained. To our best knowledge, it's the first time to estimate the contribution of anthropogenic sources -

302 Chinese cooking SOA and vehicle SOA in ambient air by a multilinear engine model (ME-2), through

303 creatively employs mass spectra of SOA factors to constrain the OA source apportionments, all which has

304 been implemented in biogenic SOA (Hu et al., 2016b; Zhang et al., 2017b). Due to the limitation of research

305 methods, the experiments were conducted under the oxidation conditions without other inorganic aerosol

306 seeds. In the future, it is still necessary to take further researches, for instance, use a qusi-atmospheric

307 aerosol evolution study (QUALITY) chamber to study the SOA formation under different actual oxidation

308 conditions, like high/low NO_x and so forth. According to previous studies, using some parameter

309 assumptions of vehicle exhaust, it is estimated that cooking SOA accounts for 35% of the SOA in downtown

310 Los Angeles through the model. Our research found that SOA from the urban lifestyle sources contributed

311   19% and 35% of OA in the wintertime and summertime of Shanghai, implying the need to develop control

312   measures to reduce emissions from lifestyle sources in the future.

313

314   **Supporting information**

315   Schematic depiction of the simulation and measurement system (Figure S1); Details of the mass spectra of

316   aged HOA and aged COA (Figures S2-S5); Van Krevelen diagram of POA, aged COA and aged HOA

317   (Figure S6); ME-2 source analysis during the summer observation in Shanghai (Figure S8); Experimental

318   parameters (Table S1); Mass spectra similarity analysis (Table S2-S10; Figure S7).

319   **Data availability.** The data provided in this paper can be obtained from the author upon request

320   (songguo@pku.edu.cn).

321   **Author contribution.** Wenfei Zhu, Zirui Zhang, Hui Wang, Ying Yu, Zheng Chen, Ruizhe Shen, Rui Tan,

322   Kai Song, Kefan Liu, Rongzhi Tang, Yi Liu, Yuanju Li, Wenbin Zhang, and Zhou Zhang conducted the

323   experiments. Wenfei Zhu, Zirui Zhang, Song Guo, and Min Hu analyzed the data. Shengrong Lou, Shijin

324   Shuai, Hongming Xu, Shuangde Li, Yunfa Chen, Francesco Canonaco, and Andre. S. H. Prévôt reviewed

325   and commented on the paper. Wenfei Zhu and Song Guo wrote the paper.

326   **Competing interests.** The authors declare no competing financial interest.

333   **References**

334 Alfarra, M.R., Prevot, A.S.H., Szidat, S., Sandradewi, J., Weimer, S., Lanz, V.A., Schreiber, D., Mohr, M., Baltensperger, U., 2007.
335 Identification of the mass spectral signature of organic aerosols from wood burning emissions. Environmental Science &
336 Technology 41, 5770-5777.
337 Budisulistiorini, S.H., Canagaratna, M.R., Croteau, P.L., Marth, W.J., Baumann, K., Edgerton, E.S., Shaw, S.L., Knipping, E.M.,
338 Worsnop, D.R., Jayne, J.T., Gold, A., Surratt, J.D., 2013. Real-Time Continuous Characterization of Secondary Organic
339 Aerosol Derived from Isoprene Epoxydiols in Downtown Atlanta, Georgia, Using the Aerodyne Aerosol Chemical Speciation
340 Monitor. Environmental Science & Technology 47, 5686-5694.
341 Canagaratna, M.R., Jayne, J.T., Jimenez, J.L., Allan, J.D., Alfarra, M.R., Zhang, Q., Onasch, T.B., Drewnick, F., Coe, H.,
342 Middlebrook, A., Delia, A., Williams, L.R., Trimborn, A.M., Northway, M.J., DeCarlo, P.F., Kolb, C.E., Davidovits, P., Worsnop,
343 D.R., 2007. Chemical and microphysical characterization of ambient aerosols with the aerodyne aerosol mass spectrometer.
344 Mass Spectrometry Reviews 26, 185-222.
345 Canonaco, F., Crippa, M., Slowik, J.G., Baltensperger, U., Prevot, A.S.H., 2013. SoFi, an IGOR-based interface for the efficient
346 use of the generalized multilinear engine (ME-2) for the source apportionment: ME-2 application to aerosol mass
347 spectrometer data. Atmospheric Measurement Techniques 6, 3649-3661.
348 Collier, S., Zhou, S., Kuwayama, T., Forestieri, S., Brady, J., Zhang, M., Kleeman, M., Cappa, C., Bertram, T., Zhang, Q., 2015.
349 Organic PM Emissions from Vehicles: Composition, O/C Ratio, and Dependence on PM Concentration. Aerosol Science
350 and Technology 49, 86-97.
351 Elser, M., Huang, R.-J., Wolf, R., Slowik, J.G., Wang, Q., Canonaco, F., Li, G., Bozzetti, C., Daellenbach, K.R., Huang, Y., Zhang,
352 R., Li, Z., Cao, J., Baltensperger, U., El-Haddad, I., Prevot, A.S.H., 2016. New insights into PM2.5 chemical composition and
353 sources in two major cities in China during extreme haze events using aerosol mass spectrometry. Atmospheric Chemistry
354 and Physics 16, 3207-3225.
355 Ge, X., Li, L., Chen, Y., Chen, H., Wu, D., Wang, J., Xie, X., Ge, S., Ye, Z., Xu, J., 2017. Aerosol characteristics and sources in
356 Yangzhou, China resolved by offline aerosol mass spectrometry and other techniques. Environmental Pollution 225, 74-85.
357 Guo, S., Hu, M., Guo, Q., Zhang, X., Zheng, M., Zheng, J., Chang, C.C., Schauer, J.J., Zhang, R., 2012. Primary Sources and
358 Secondary Formation of Organic Aerosols in Beijing, China. Environmental Science & Technology 46, 9846-9853.
359 Guo, S., Hu, M., Zamora, M.L., Peng, J., Shang, D., Zheng, J., Du, Z., Wu, Z., Shao, M., Zeng, L., Molina, M.J., Zhang, R., 2014.
360 Elucidating severe urban haze formation in China. Proceedings of the National Academy of Sciences of the United States of
361 America 111, 17373-17378.
362 He, L.Y., Huang, X.F., Xue, L., Hu, M., Lin, Y., Zheng, J., Zhang, R., Zhang, Y.H., 2011. Submicron aerosol analysis and organic
363 source apportionment in an urban atmosphere in Pearl River Delta of China using high - resolution aerosol mass
364 spectrometry. Journal of Geophysical Research Atmospheres 116, -.
365 He, L.Y., Lin, Y., Huang, X.F., Guo, S., Xue, L., Su, Q., Hu, M., Luan, S.J., Zhang, Y.H., 2010. Characterization of high-resolution
366 aerosol mass spectra of primary organic aerosol emissions from Chinese cooking and biomass burning. Atmospheric
367 Chemistry and Physics 10, 11535-11543.
368 Hu, W., Hu, M., Hu, W., Jimenez, J.L., Yuan, B., Chen, W., Wang, M., Wu, Y., Chen, C., Wang, Z., 2016a. Chemical composition,
369 sources, and aging process of submicron aerosols in Beijing: Contrast between summer and winter. Journal of Geophysical
370 Research Atmospheres 121, 1955-1977.
371 Hu, W., Hu, M., Hu, W.W., Zheng, J., Chen, C., Wu, Y., Guo, S., 2017. Seasonal variations in high time-resolved chemical
372 compositions, sources, and evolution of atmospheric submicron aerosols in the megacity Beijing. Atmospheric Chemistry &
373 Physics 17, 9979-10000.
374 Hu, W., Palm, B.B., Day, D.A., Campuzano-Jost, P., Krechmer, J.E., Peng, Z., de Sa, S.S., Martin, S.T., Alexander, M.L.,
375 Baumann, K., Hacker, L., Kiendler-Scharr, A., Koss, A.R., de Gouw, J.A., Goldstein, A.H., Seco, R., Sjostedt, S.J., Park, J.-H.,
376 Guenther, A.B., Kim, S., Canonaco, F., Prevot, A.S.H., Brune, W.H., Jimenez, J.L., 2016b. Volatility and lifetime against OH
377 heterogeneous reaction of ambient isoprene-epoxydiols-derived secondary organic aerosol (IEPOX-SOA). Atmospheric
378 Chemistry and Physics 16, 11563-11580.

379 Huang, X.F., He, L.Y., Hu, M., Canagaratna, M.R., Kroll, J.H., Ng, N.L., Zhang, Y.H., Lin, Y., Xue, L., Sun, T.L., 2011.
380 Characterization of submicron aerosols at a rural site in Pearl River Delta of China using an Aerodyne High-Resolution
381 Aerosol Mass Spectrometer. Atmospheric Chemistry & Physics 11, 1865-1877.

382 Kaltsonoudis, C., Kostenidou, E., Louvaris, E., Psichoudaki, M., Tsiligiannis, E., Florou, K., Liangou, A., Pandis, S.N., 2017.
383 Characterization of fresh and aged organic aerosol emissions from meat charbroiling. Atmospheric Chemistry and Physics
384 17, 7143-7155.

385 Katragadda, H.R., Fullana, A., Sidhu, S., Carbonell-Barrachina, A.A., 2010. Emissions of volatile aldehydes from heated
386 cooking oils. Food Chemistry 120, 59-65.

387 Kim, H., Zhang, Q., Bae, G.-N., Kim, J.Y., Lee, S.B., 2017. Sources and atmospheric processing of winter aerosols in Seoul,
388 Korea: insights from real-time measurements using a high-resolution aerosol mass spectrometer. Atmospheric Chemistry
389 and Physics 17, 2009-2033.

390 Klein, F., Platt, S.M., Farren, N.J., Detournay, A., Bruns, E.A., Bozzetti, C., Daellenbach, K.R., Kilic, D., Kumar, N.K., Pieber, S.M.,
391 Slowik, J.G., Temime-Roussel, B., Marchand, N., Hamilton, J.F., Baltensperger, U., Prevot, A.S.H., El Haddad, I., 2016.
392 Characterization of Gas-Phase Organics Using Proton Transfer Reaction Time-of-Flight Mass Spectrometry: Cooking
393 Emissions. Environmental Science & Technology 50, 1243-1250.

394 Kostenidou, E., Lee, B.-H., Engelhart, G.J., Pierce, J.R., Pandis, S.N., 2009. Mass Spectra Deconvolution of Low, Medium, and
395 High Volatility Biogenic Secondary Organic Aerosol. Environmental Science & Technology 43, 4884-4889.

396 Li, J., Liu, Q., Li, Y., Liu, T., Huang, D., Zheng, J., Zhu, W., Hu, M., Wu, Y., Lou, S., Hallquist, A.M., Hallquist, M., Chan, C.K.,
397 Canonaco, F., Prevot, A.S.H., Fung, J.C.H., Lau, A.K.H., Yu, J.Z., 2019. Characterization of Aerosol Aging Potentials at
398 Suburban Sites in Northern and Southern China Utilizing a Potential Aerosol Mass (Go:PAM) Reactor and an Aerosol Mass
399 Spectrometer. Journal of Geophysical Research-Atmospheres 124, 5629-5649.

400 Li, Y.J., Sun, Y., Zhang, Q., Li, X., Li, M., Zhou, Z., Chan, C.K., 2017. Real-time chemical characterization of atmospheric
401 particulate matter in China: A review. Atmospheric Environment 158, 270-304.

402 Liu, T., Li, Z., Chan, M., Chan, C.K., 2017. Formation of secondary organic aerosols from gas-phase emissions of heated
403 cooking oils. Atmospheric Chemistry and Physics 17, 7333-7344.

404 Liu, T., Wang, Z., Wang, X., Chan, C.K., 2018. Primary and secondary organic aerosol from heated cooking oil emissions.
405 Atmospheric Chemistry and Physics 18, 11363-11374.

406 Louvaris, E.E., Karnezi, E., Kostenidou, E., Kaltsonoudis, C., Pandis, S.N., 2017. Estimation of the volatility distribution of
407 organic aerosol combining thermodenuder and isothermal dilution measurements. Atmospheric Measurement Techniques
408 10, 3909-3918.

409 Mohr, C., DeCarlo, P.F., Heringa, M.F., Chirico, R., Slowik, J.G., Richter, R., Reche, C., Alastuey, A., Querol, X., Seco, R.,
410 Penuelas, J., Jimenez, J.L., Crippa, M., Zimmermann, R., Baltensperger, U., Prevot, A.S.H., 2012. Identification and
411 quantification of organic aerosol from cooking and other sources in Barcelona using aerosol mass spectrometer data.
412 Atmospheric Chemistry and Physics 12, 1649-1665.

413 Paatero, P., 1999. The multilinear engine - A table-driven, least squares program for solving multilinear problems,
414 including the n-way parallel factor analysis model. Journal of Computational and Graphical Statistics 8, 854-888.

415 Paatero, P., Hopke, P.K., 2003. Discarding or downweighting high-noise variables in factor analytic models. Analytica
416 Chimica Acta 490, 277-289.

417 Peng, Z., Day, D.A., Ortega, A.M., Palm, B.B., Hu, W., Stark, H., Li, R., Tsigaridis, K., Brune, W.H., Jimenez, J.L., 2016. Non-OH
418 chemistry in oxidation flow reactors for the study of atmospheric chemistry systematically examined by modeling.
419 Atmospheric Chemistry and Physics 16, 4283-4305.

420 Presto, A.A., Gordon, T.D., Robinson, A.L., 2014. Primary to secondary organic aerosol: evolution of organic emissions from
421 mobile combustion sources. Atmospheric Chemistry and Physics 14, 5015-5036.

422 Qin, Y.M., Tan, H.B., Li, Y.J., Schurman, M.I., Li, F., Canonaco, F., Prevot, A.S.H., Chan, C.K., 2017. Impacts of traffic emissions
423 on atmospheric particulate nitrate and organics at a downwind site on the periphery of Guangzhou, China. Atmospheric
424 Chemistry and Physics 17, 10245-10258.

425   Robinson, A.L., Donahue, N.M., Shrivastava, M.K., Weitkamp, E.A., Sage, A.M., Grieshop, A.P., Lane, T.E., Pierce, J.R., Pandis,
426   S.N., 2007. Rethinking organic aerosols: Semivolatile emissions and photochemical aging. Science 315, 1259-1262.

427   Schauer, J.J., Kleeman, M.J., Cass, G.R., Simoneit, B.R.T., 2002. Measurement of emissions from air pollution sources. 4.
428   C-1-C-27 organic compounds from cooking with seed oils. Environmental Science & Technology 36, 567-575.

429   Sun, J., Zhang, Q., Canagaratna, M.R., Zhang, Y., Ng, N.L., Sun, Y., Jayne, J.T., Zhang, X., Zhang, X., Worsnop, D.R., 2010.
430   Highly time-and size-resolved characterization of submicron aerosol particles in Beijing using an Aerodyne Aerosol Mass
431   Spectrometer. Atmospheric Environment 44, 131-140.

432   Sun, Y., Du, W., Fu, P., Wang, Q., Li, J., Ge, X., Zhang, Q., Zhu, C., Ren, L., Xu, W., 2016. Primary and secondary aerosols in
433   Beijing in winter: sources, variations and processes. Atmospheric Chemistry & Physics 16, 1-41.

434   Sun, Y., Jiang, Q., Wang, Z., Fu, P., Li, J., Yang, T., Yin, Y., 2014. Investigation of the sources and evolution processes of
435   severe haze pollution in Beijing in January 2013. Journal of Geophysical Research Atmospheres 119, 4380-4398.

436   Sun, Y., Xu, W., Zhang, Q., Jiang, Q., Canonaco, F., Prévôt, A.S., Fu, P., Li, J., Jayne, J., Worsnop, D.R., 2018. Source
437   apportionment of organic aerosol from two-year highly time-resolved measurements by an aerosol chemical speciation
438   monitor in Beijing, China. Atmospheric Chemistry and Physics Discussions, 1-33.

439   Ulbrich, I., Canagaratna, M., Zhang, Q., Worsnop, D., Jimenez, J., 2009. Interpretation of organic components from positive
440   matrix factorization of aerosol mass spectrometric data. Atmospheric Chemistry & Physics 9.

441   Wang, H., Xiang, Z., Wang, L., Jing, S., Lou, S., Tao, S., Liu, J., Yu, M., Li, L., Lin, L., Chen, Y., Wiedensohler, A., Chen, C., 2018.
442   Emissions of volatile organic compounds (VOCs) from cooking and their speciation: A case study for Shanghai with
443   implications for China. Science of the Total Environment 621, 1300-1309.

444   Wang, J., Ge, X., Chen, Y., Shen, Y., Zhang, Q., Sun, Y., Xu, J., Ge, S., Yu, H., Chen, M., 2016. Highly time-resolved urban
445   aerosol characteristics during springtime in Yangtze River Delta, China: insights from soot particle aerosol mass
446   spectrometry. Atmospheric Chemistry and Physics 16, 9109-9127.

447   Wenfei, Z., Song, G., Shengrong, L., Hui, W., Ying, Y., Weizhao, X., Yucun, L., Zhen, C., Xiaofeng, H., Lingyan, H., Limin, Z.,
448   Shiyi, C., Min, H., 2020. A novel algorithm to determine the scattering coefficient of ambient organic aerosols.
449   Environmental Pollution.

450   Xu, J., Shi, J., Zhang, Q., Ge, X., Canonaco, F., Prévôt, A.S., Vonwiller, M., Szidat, S., Ge, J., Ma, J., 2016. Wintertime organic
451   and inorganic aerosols in Lanzhou, China: sources, processes, and comparison with the results during summer.
452   Atmospheric Chemistry and Physics 16, 14937-14957.

453   Xu, W., Han, T., Wei, D., Wang, Q., Chen, C., Jian, Z., Zhang, Y., Jie, L., Fu, P., Wang, Z., 2017. Effects of Aqueous-phase and
454   Photochemical Processing on Secondary Organic Aerosol Formation and Evolution in Beijing, China. Environmental
455   Science & Technology 51, 762.

456   Xu, W., He, Y., Qiu, Y., Chen, C., Xie, C., Lei, L., Li, Z., Sun, J., Li, J., Fu, P., Wang, Z., Worsnop, D., Sun, Y., 2020. Mass spectral
457   characterization of primary emissions and implications in source apportionment of organic aerosol. Atmospheric
458   Measurement Techniques 13, 3205-3219.

459   Ying, Y.A.B., Hui, W.A., A, T.W., Kai, S.A., A, T.T., A, Z.W., C, Y.G., A, H.D., A, S.C., D, L.Z.A.B., 2020. Elucidating the importance
460   of semi-volatile organic compounds to secondary organic aerosol formation at a regional site during the EXPLORE-YRD
461   campaign - ScienceDirect. Atmospheric Environment.

462   Zhang, Q., Jimenez, J.L., Canagaratna, M.R., Ulbrich, I.M., Ng, N.L., Worsnop, D.R., Sun, Y., 2011. Understanding atmospheric
463   organic aerosols via factor analysis of aerosol mass spectrometry: a review. Analytical & Bioanalytical Chemistry 401,
464   3045-3067.

465   Zhang, X., Zhang, Y., Sun, J., Yu, Y., Canonaco, F., Prevot, A.S.H., Li, G., 2017a. Chemical characterization of submicron
466   aerosol particles during wintertime in a northwest city of China using an Aerodyne aerosol mass spectrometry.
467   Environmental Pollution 222, 567-582.

468   Zhang, Y., Tang, L., Sun, Y., Favez, O., Canonaco, F., Albinet, A., Couvidat, F., Liu, D., Jayne, J.T., Wang, Z., Croteau, P.L.,
469   Canagaratna, M.R., Zhou, H.-c., Prevot, A.S.H., Worsnop, D.R., 2017b. Limited formation of isoprene epoxidiols-derived
470   secondary organic aerosol under NOx-rich environments in Eastern China. Geophysical Research Letters 44, 2035-2043.

471   Zhang, Y.J., Tang, L.L., Wang, Z., Yu, H.X., Sun, Y.L., Liu, D., Qin, W., Zhang, H.L., Zhou, H.C., 2014. Insights into
472   characteristics, sources and evolution of submicron aerosols during harvest seasons in Yangtze River Delta (YRD) region,
473   China. Atmospheric Chemistry & Physics 14, 9109-9154.
474   Zhang, Z., Zhu, W., Hu, M., Wang, H., Chen, Z., Shen, R., Yu, Y., Tan, R., Guo, S., 2020. Secondary Organic Aerosol from
475   Typical Chinese Domestic Cooking Emissions. Environmental Science & Technology Letters.
476   Zhou, W., Wang, Q., Zhao, X., Xu, W., Chen, C., Du, W., Zhao, J., Canonaco, F., Prevot, A.S.H., Fu, P., Wang, Z., Worsnop, D.R.,
477   Sun, Y., 2018. Characterization and source apportionment of organic aerosol at 260 m on a meteorological tower in Beijing,
478   China. Atmospheric Chemistry and Physics 18, 3951-3968.

479